*Clays and Clay Minerals*, Vol. 36, No. 1, 47–60, 1988.

# TRANSMISSION ELECTRON MICROSCOPE STUDY OF BIOTITE WEATHERING

JILLIAN F. BANFIELD[1] AND RICHARD A. EGGLETON

Department of Geology, Australian National University
P.O. Box 4, Canberra, A.C.T. 2601, Australia

**Abstract**—Transmission electron microscopy suggests that biotite transforms to vermiculite primarily by direct structural modification, involving the replacement of $K^+$ by hydrated interlayer cations, and only minor reorganization of the 2:1 layer. A second relatively uncommon mechanism appears to involve redistribution of components from two biotite sheets to form a single vermiculite layer. Distortion of the surrounding structure initially inhibits growth of vermiculite in the surrounding biotite, and promotes the propagation of vermiculite layers in opposite directions. This phenomenon may contribute to the development of relatively regular, widely spaced interstratifications of biotite and vermiculite. Additional components and space are provided by the dissolution of biotite where access of solutions is greater.

During weathering, biotite and vermiculite become increasingly replaced by kaolinite, which crystallizes epitactically onto existing layers, and goethite, which develops from a poorly crystalline iron oxyhydroxide precursor to form oriented laths. In areas parts of strongly weathered samples kaolinite and goethite appear to develop in proportions consistent with a reaction that conserves both Al and Fe.

**Key Words**—Biotite, Goethite, Granodiorite, Kaolinite, Lattice-fringe images, Transmission electron microscopy, Vermiculite, Weathering.

## INTRODUCTION

Many workers have studied the process and products of biotite weathering by observing both naturally altered materials and mica weathered artificially in the laboratory. This topic has attracted particular attention because biotite is an important source of K in soils; hence, factors affecting the breakdown of this mineral exert some influence on soil fertility. Published accounts of the development of weathering products under a range of environmental conditions include those of Walker (1949), Coleman *et al.* (1963), Wilson (1966, 1970), Meunier and Velde (1979), and Gilkes and Suddhiprakarn (1979). These authors identified many minerals that were formed as a result of biotite weathering, including interstratified biotite and vermiculite, chlorite/vermiculite, vermiculite, kaolin-group minerals, iron and titanium oxides, and gibbsite. Montmorillonite was identified by MacEwan (1953) as an alteration product of biotite in poorly drained soils.

The variety of minerals observed in such weathering products has led to the suggestion that biotite weathers to different end products under different weathering conditions (Wilson, 1966). On the other hand, Meunier and Velde (1979) found that although the final products of biotite weathering are always the same, the nature of the intermediate mineral assemblage varies due to differences in the chemical environment, such as differences in the composition of the altering fluid.

The development of oriented alteration products was noted by Wilson (1966), who described the epitactic crystallization of gibbsite and kaolinite onto biotite, and by Gilkes and Suddhiprakarn (1979), who reported that goethite crystallizes with *Z* parallel to biotite *Y*, presumably by nucleation of the iron-oxygen octahedral chains of goethite parallel to octahedral strips in biotite.

Norrish (1973) summarized much of the work on artificially weathered micas. For example, the ease of removal of K has been explained in terms of the orientation of the OH bond. Norrish described the retarding effect of large monovalent cations (particularly K) in solution on the reaction, and noted that charge reduction can be attributed to oxidation of $Fe^{2+}$.

In this study we describe the weathering of igneous biotite, using transmission electron microscopy to image the various alteration products. We show evidence for a two-stage process, first, the development of interstratified biotite/vermiculite without an overall volume increase, and only requiring addition of $H_2O$, and second the formation of kaolinite-goethite, with an estimated 20% volume decrease, conserving Al and Fe.

## EXPERIMENTAL

### *Samples*

Biotite weathering was examined from three profiles through weathered granitoids exposed in road cuts in the Snowy Mountains of New South Wales, Australia. Most of the work reported here is on samples from the Bullenbalong Granodiorite, exposed on the Snowy Mountains Highway east of Lake Jindabyne (Figure 1).

[1] Present address: Department of Earth and Planetary Sciences, The Johns Hopkins University, Baltimore, Maryland 21218

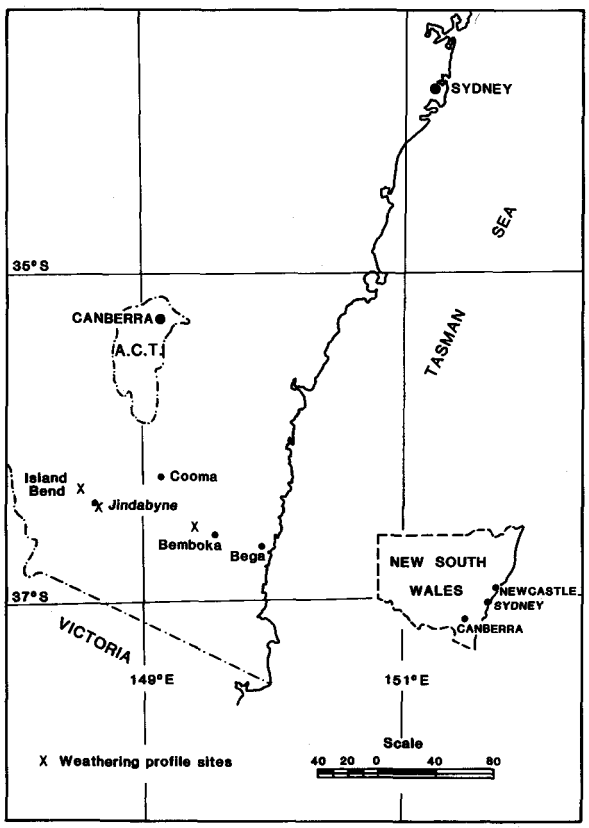


Figure 1. Map of granodiorite sample localities, New South Wales.

The fresh rock contains 18% red-brown biotite that shows very slight chloritization, 32% plagioclase (zoned from $An_{13}$ to $An_{50}$), 12% K-feldspar, and 35% quartz, with accessory muscovite, apatite, monazite, zircon, tourmaline, and opaque minerals. The rock is weakly foliated. A second biotite was examined from the Bemboka Granodiorite, located near the top of Brown Mountain between the towns of Cooma and Bemboka. Biotite in the fresh rock is partly chloritized and occludes epidote and clusters of fine-grained sphene crystals, as well as magnetite and prehnite. Biotite comprises 10% of the rock, which also contains 32% plagioclase ($An_{11-48}$), 3% amphibole, 16% K-feldspar, and 35% quartz. Accessory minerals are allanite, zircon, apatite, and magnetite. The third profile examined was through the Island Bend Granodiorite in the Snowy Mountains. The fresh rock contains 9% biotite somewhat altered to chlorite, epidote, and sphene, 44% plagioclase ($An_{20-50}$), 12% K-feldspar, and 34% quartz. Accessory minerals are amphibole, apatite, and magnetite.

For each of the profiles examined, six samples were taken from progressively weathered shells around a solid, fresh, rounded core-stone. The most weathered samples still retained the original igneous texture and remained coherent if handled carefully. Extent of weathering was gauged by whole rock density, which conformed to estimates of weathering intensity based on color, position in the profile relative to the core-stone, and coherence. References below to samples being more weathered or less weathered refer to these criteria.

### *Methods*

Copper grids 2 or 3 mm in diameter were glued with epoxy resin to fresh and weathered biotite crystals in petrographic thin sections glued to a glass slide with thermo-plastic Aremco Crystalbond. The grids and crystals were cut free and lifted from the thin section after heating to 80°C, then further thinned to electron transparency by Ar-ion bombardment at an angle of 22° to the section surface, using 4–5 kV in a vacuum of $10^{-4}$ torr.

The ion-thinned samples were examined in a JEOL 100CX transmission electron microscope (TEM) with a side-entry double-tilt goniometer, operating at 100 kV, and a JEOL 200CX TEM fitted with an ultra high resolution, top-entry stage, operating at 200 kV. The identity of alteration products was confirmed using a JEOL 100CX scanning-transmission electron microscope (STEM) equipped with an energy-dispersive X- ray detector, allowing qualitative chemical analysis of very small areas of material ($<1000$ Å$^2$). Weathered biotite samples were examined by X-ray powder diffraction (XRD) with a Philips goniometer and 1010 generator, CoK$\alpha$ radiation and a graphite monochromator, operated at 40 kV and 20 mA. Quantitative compositions of biotite, chlorite, and alteration products were obtained using an energy dispersive Technisch Physich Dienst electron microprobe. $Fe^{2+}/Fe^{3+}$ ratios in biotite were obtained by dichromate titration of dissolved mineral separates (E. Kiss, analyst).

Chemical analyses of whole rock samples were made by X-ray fluorescence analysis (Norrish and Chappell, 1977). Ferrous/ferric ratios were determined by titration against $K_2Cr_2O_7$ after digestion in HF + $H_2SO_4$, and water and $CO_2$ were analyzed by absorption on $P_2O_5$ and NaOH, respectively.

Whole rock densities were measured by Archimedes' principle on paraffin-coated specimens.

## RESULTS

### *Optical microscopy*

Examination of biotite with a petrographic microscope indicated that although this mineral begins to weather relatively early compared with other granitic minerals, alteration initially proceeds slowly. It is not until quite late in weathering that replacement by secondary products becomes pronounced.

Biotite in samples J2 and J3 shows sporadic development of vermiculite as evidenced by the presence of paler lamellae parallel to (001). This stage of weath-

https://doi.org/10.1346/CCMN.1988.0360107 Published online by Cambridge University Press

Table 1. Chemical analyses (wt. %) of fresh and weathered Bullenbalong Granodiorite near Jindabyne, New South Wales, Australia.

| | J1 | J2 | J3 | J4 | J5 | J6 |
|---|---|---|---|---|---|---|
| $SiO_2$ | 70.09 | 69.81 | 69.73 | 68.48 | 67.85 | 68.90 |
| $TiO_2$ | 0.56 | 0.54 | 0.55 | 0.54 | 0.52 | 0.54 |
| $Al_2O_3$ | 14.05 | 13.91 | 14.04 | 14.13 | 14.43 | 14.48 |
| $Fe_2O_3$ | 0.34 | 1.39 | 0.97 | 3.37 | 3.71 | 3.66 |
| FeO | 3.41 | 2.38 | 2.77 | 0.62 | 0.27 | 0.40 |
| MnO | 0.06 | 0.05 | 0.05 | 0.04 | 0.03 | 0.05 |
| MgO | 1.63 | 1.58 | 1.65 | 1.47 | 1.51 | 1.49 |
| CaO | 2.21 | 1.74 | 1.63 | 1.13 | 0.63 | 1.22 |
| $Na_2O$ | 2.29 | 2.21 | 2.30 | 1.98 | 1.76 | 1.85 |
| $K_2O$ | 3.80 | 3.88 | 4.13 | 3.90 | 4.28 | 3.58 |
| $P_2O_5$ | 0.10 | 0.09 | 0.10 | 0.09 | 0.04 | 0.07 |
| S | 0.04 | 0.01 | 0.01 | 0.01 | 0.01 | 0.01 |
| $H_2O+$ | 1.21 | 1.42 | 1.36 | 2.09 | 2.83 | 2.39 |
| $H_2O-$ | 0.14 | 0.36 | 0.24 | 0.91 | 1.11 | 0.59 |
| $CO_2$ | 0.33 | 0.13 | 0.08 | 0.15 | 0.28 | 0.58 |
| O = S | 0.02 | 0.01 | 0.01 | | | |
| Total | 100.23 | 99.50 | 99.59 | 98.91 | 99.25 | 99.81 |
| | | | Minor elements (ppm) | | | |
| Ba | 480 | 490 | 490 | 490 | 475 | 455 |
| Rb | 184 | 187 | 195 | 168 | 173 | 180 |
| Sr | 117 | 108 | 106 | 94 | 75 | 93 |
| Zr | 174 | 180 | 179 | 177 | 154 | 169 |
| Y | 32 | 31 | 32 | 30 | 24 | 28 |
| La | 29 | 27 | 25 | 32 | 29 | 30 |
| Ce | 67 | 63 | 57 | 66 | 51 | 62 |
| V | 68 | 71 | 70 | 89 | 89 | 85 |
| Cr | 35 | 35 | 37 | 44 | 43 | 42 |
| Pb | 27 | 26 | 26 | 28 | 25 | 27 |
| Ni | 12 | 12 | 12 | 12 | 12 | 13 |
| Cu | 13 | 12 | 8 | 17 | 14 | 10 |
| Zn | 58 | 58 | 60 | 66 | 58 | 54 |
| Nb | 12 | 12 | 12 | 12 | 10 | 11 |

ering is here called the biotite-vermiculite stage. In samples J4–J6 the biotite is progressively more disrupted. Granular, dark-colored iron oxyhydroxides and kaolinite occupy cracks and holes. Biotites from the other profiles examined show a similar sequence of alteration features. This stage is referred to as the kaolinite-goethite stage.

*Whole rock chemistry*

Bulk chemical analyses for samples J1–J6 are presented in Table 1. The main features relevant to this study are the sharp increases in the $Fe_2O_3$:FeO ratio and the total water content between samples J3 and J4. These changes mark the transition from the biotite-vermiculite stage to the kaolinite-goethite stage noted optically.

*X-ray powder diffraction*

Figure 2 shows XRD traces from biotite extracted from successively more weathered Bullenbalong Granodiorite and for the same samples after heating to 350°C. In the least weathered sample shown (J3), vermiculite is the only alteration product developed in sufficient abundance to be detected. In subsequent stages (samples J4–J6), kaolinite becomes increasingly abundant, as does vermiculite (and goethite, not shown). In the most weathered sample (J6), an asymmetric broadening of the 10-Å peak toward the 14-Å peak and a discrete 12-Å peak was recognized. Halloysite appears to be a minor component of the weathering assemblage; it was identified using the formamide treatment advocated by Churchman *et al.* (1984). Goethite peaks were broad and poorly defined.

*Mineral chemistry*

Electron microprobe analyses of biotite, vermiculite, and kaolinite are presented in Table 2. Calculation of mineral formulae is based on +44 cation charge for biotite and vermiculite and +28 for kaolinite. All iron is assumed to be ferric in the weathered products (vermiculite and kaolinite). Goethite aggregates and the kaolinites from Island Bend and Jindabyne were too small for analysis by electron microprobe. Analytical electron microscopy (AEM) of goethites showed only the presence of iron.

https://doi.org/10.1346/CCMN.1988.0360107 Published online by Cambridge University Press

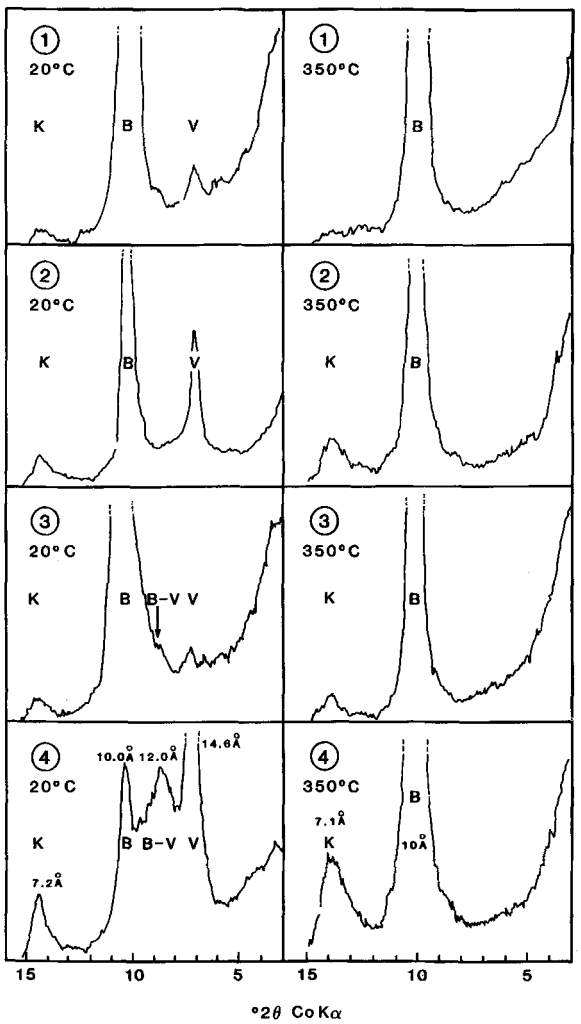


Figure 2. X-ray powder diffractometer patterns of biotites in samples J3, J4, J5, J6, run at 20°C and after heating to 350°C. B = biotite, K = kaolinite, V = vermiculite, B-V = biotite/vermiculite interstratification.

*Transmission electron microscopy*

The description of TEM from a sample in which a change or process has been arrested involves some degree of interpretation based on external criteria. The assumptions used to describe the images presented here are: (1) In thin regions (<200 Å) of oriented phyllosilicate photographed at about 800 Å underfocus (estimated by the Fresnel fringe) dark areas are more electron dense than light areas (Cowley and Iijima, 1976). (2) Changes in contrast across areas showing lattice-fringe images result from small orientation changes in the crystal. (3) Reversal of contrast (black for white) is a consequence of thickness change. (4) The ratio of 14- Å to 10-Å layers increases with increased weathering.

Weathering is a process taking place through time,

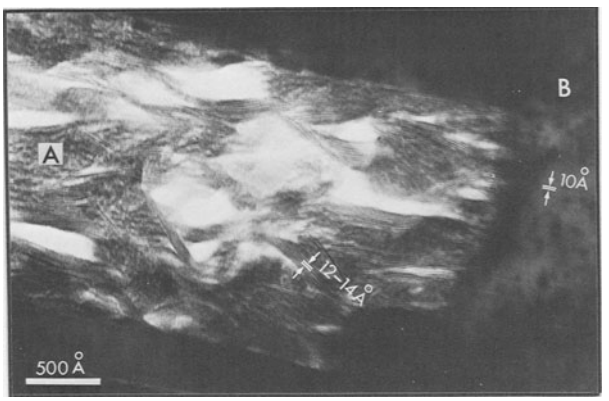


Figure 3. Transmission electron micrograph showing etch pit in biotite (B) containing poorly or noncrystalline material (A) and curving strips of phyllosilicate mineral.

whereas the micrographs depict only one instant. Spatial relationships were used to interpret temporal relationships in the same way that a half-open zipper reveals a process: the open part shows how the closed part will look later in time. The analogy is limited, because zip-fasteners can close more readily than vermiculite converts to biotite during weathering.

*Early stage of weathering.* TEMs of biotite from the weakly weathered granodiorites are characterized by sporadic, elongate etch pits, their long dimensions parallel to the mica sheets. Noncrystalline material and wispy 12- to 14-Å phyllosilicates occur in these etch pits (Figure 3). Commonly, the etch pits extend a considerable distance (as much as 1 $\mu$m) through the biotite (Figure 4).

Figures 5 shows additional features of this stage of weathering: narrow zones between biotite layers having low contrast, terminating biotite layers and distortion of the remaining biotite layers.

*Biotite-vermiculite stage.* Samples taken from slightly more weathered rock show, in addition to local regions of etch pits, large areas of interstratified 10-Å and 14- Å phyllosilicates, identified by comparison with the XRD data as well as by direct imaging of the cation sheets, as interstratified biotite/vermiculite. The TEM features of this stage of weathering are shown in Figures 6–12.

The distinction between biotite and vermiculite is clearly shown in Figure 6b and, at lower resolution, in Figure 6c. In Figure 6b, the 2:1 layer is imaged as three dark bands, the octahedral sheet being slightly darker than the tetrahedral sheets on either side. In the same illustration, hydrated interlayers show as paler strips between 2:1 layers. In Figure 6c (and comparable photographs in Figures 8, 10, and 12), the components of the 2:1 layers are not resolved, but the 2:1 layer is distinguished from the interlayer by contrast. Figures 6b and 6c were photographed parallel to (001), whereas

https://doi.org/10.1346/CCMN.1988.0360107 Published online by Cambridge University Press

Figure 6a was taken parallel to [110] and shows 4.5-Å ($1\bar{1}0$) lattice fringes, in addition to (001) fringes.

As illustrated in Figure 6b, the transformation from biotite to vermiculite occurs over only a few Ångstroms, with very little disruption of the surrounding structure. The 2:1 layer of biotite is apparently continuous with that of vermiculite, suggesting that it was inherited almost intact. The layers immediately adjacent to the expanding layer remain attached, and bend around the distortion. This flexure is commonly transferred through the structure for a few unit cells (often fewer than 10) to where another biotite has converted to vermiculite extending in the opposite direction.

A second, less common mechanism is also visible; it apparently involves the conversion of two biotite layers to one vermiculite. In Figure 7b, the very gradual reduction of the second biotite sheet and the apparent continuity of the reduced layer with the vermiculite sheet indicate that one vermiculite sheet has actually replaced two biotite sheets. The presence of the second biotite sheet before the appearance of the vermiculite (Figure 7a) can not be firmly established, as vermiculite may simply have developed by the first mechanism at an edge dislocation. The dislocation could have provided a pathway for the introduction of cations and water, and thus focused alteration.

The presence of a brighter interlayer region in electron micrographs of biotite before replacement by vermiculite was observed in some samples and may be due to an increase in layer width from 10 to 12 Å (Figure 8).

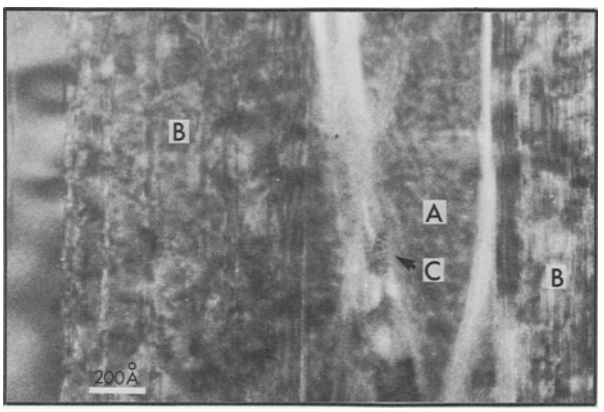


Figure 4. Transmission electron micrograph showing channel in biotite (B) bounded by {001} containing noncrystalline material (A) and poorly crystalline clay mineral (C).

The extensive areas of biotite/vermiculite shown in Figure 9 reveal a tendency for vermiculite layers to be separated from each other by four or five biotite layers, and that biotite layers are kinked where vermiculite layers terminate. Commonly the kink is absent where a second vermiculite layer extends in the opposite di-

Table 2. Electron microprobe analyses (wt. %) and structural formulae of biotite, vermiculite, and kaolinite from weathered granodiorite.

| | Biotite | | | Vermiculite | | | Kaolinite |
|---|---|---|---|---|---|---|---|
| | I.B. | Jind | Bem | I.B. | Jind | Bem | Bem |
| $SiO_2$ | 36.87 | 34.96 | 37.03 | 36.02 | 33.68 | 35.17 | 45.92 |
| $TiO_2$ | 2.85 | 3.29 | 3.75 | 2.26 | 0.21 | 0.0 | 0.0 |
| $Al_2O_3$ | 15.54 | 19.18 | 13.67 | 20.98 | 19.16 | 27.47 | 38.33 |
| $Fe_2O_3$ | 5.50 | 2.18 | — | 13.06[1] | 25.38[1] | 15.73[1] | 1.55[1] |
| FeO | 11.69 | 19.35 | 24.09[2] | — | — | — | — |
| MnO | 0.56 | 0.10 | 0.19 | 0.47 | 0.31 | 0.16 | 0.0 |
| MgO | 12.54 | 8.37 | 8.85 | 12.07 | 9.96 | 5.88 | 0.17 |
| CaO | — | — | 0.15 | 0.84 | 0.61 | 0.0 | 0.0 |
| $K_2O$ | 10.48 | 10.32 | 9.24 | 0.45 | 0.36 | 0.15 | 0.40 |
| Total | 96.05 | 97.75 | 97.00 | 86.18 | 89.67 | 84.56 | 86.37 |
| Si | 5.59 | 5.28 | 5.68 | 5.54 | 5.50 | 5.31 | 1.99 |
| $Al^{IV}$ | 2.41 | 2.72 | 2.32 | 2.46 | 2.50 | 2.69 | — |
| Ti | 0.32 | 0.37 | 0.43 | 0.26 | 0.03 | 0.0 | — |
| $Al^{VI}$ | 0.34 | 0.67 | 0.15 | 1.30 | 0.93 | 2.20 | 1.96 |
| $Fe^{3+}$ | 0.60 | 0.25 | 3.09 | 1.68 | 2.89 | 1.79 | 0.05 |
| $Fe^{2+}$ | 1.48 | 2.45 | — | — | — | — | 0.05 |
| Mn | 0.07 | 0.01 | 0.02 | 0.06 | 0.04 | 0.02 | — |
| Mg | 2.83 | 1.88 | 2.02 | 2.77 | 2.26 | 1.32 | — |
| Ca | 0.0 | 0.0 | 0.02 | 0.14 | 0.09 | 0.0 | — |
| K | 2.03 | 1.99 | 1.81 | 0.09 | 0.08 | 0.03 | — |

I.B. = Island Bend Granodiorite, Snowy Mountains, New South Wales.
Jind = Bullenbalong Granodiorite, Lake Jindabyne, New South Wales.
Bem = Bemboka Granodiorite, Bemboka, New South Wales.
[1] Fe in alteration product assumed to be ferric.
[2] Ferric : ferrous ratio not determined.

https://doi.org/10.1346/CCMN.1988.0360107 Published online by Cambridge University Press

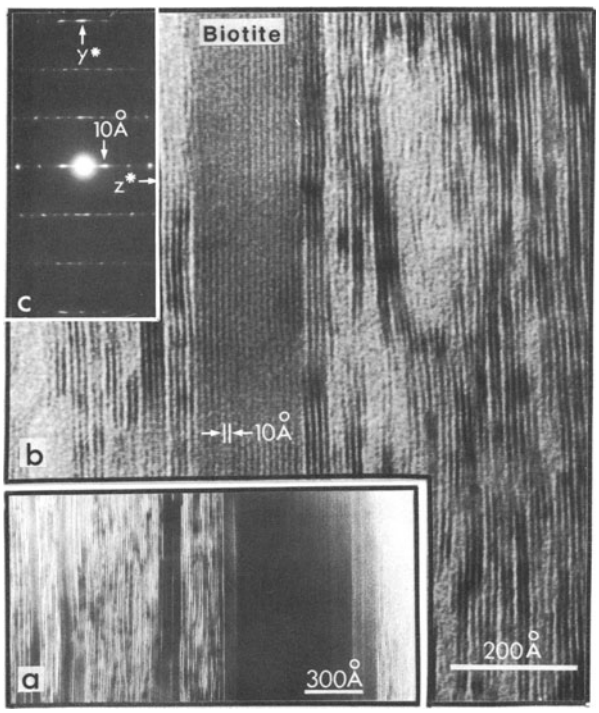


Figure 5. Lattice-fringe images of (a) region of early biotite alteration; (b) same area enlarged, showing irregularity and separation of biotite layers. Low contrast areas probably result from electron beam damage; (c) selected area electron diffraction pattern.

rection to the first. Figure 10 shows a drawing of this arrangement, with the kink in the biotite layers emphasized by arrows, comparable to the short lines drawn on the micrograph of Figure 9.

Extensive zones of vermiculite were generally not observed in the weathering sequence examined. Rather, biotite weathered to interstratified biotite/vermiculite (B/V), which displays some regularity in the way the layers alternate (Figures 11 and 12). Increased weathering correlates with an increase in the proportion of vermiculite layers and generally with an increase in the regularity of interlayering.

As shown in Figure 11, sequences of biotite-vermiculite-biotite (BVB) can be recognized, separated from adjacent BVB sets by a brighter interlayer region. Only rarely was the sequence vermiculite-vermiculite (VV) observed in this stage of alteration. Regular 1:1 interstratification was also observed (see, for example, right side of Figure 11).

*Kaolinite-goethite stage.* Kaolinite and goethite are minor constituents of the assemblage of weathering products in the earlier stages of weathering. In the later stages, however, these minerals are the dominant products, apparently replacing vermiculite as well as biotite. This stage of weathering appears to have resulted in the destruction of most of the remaining biotite.

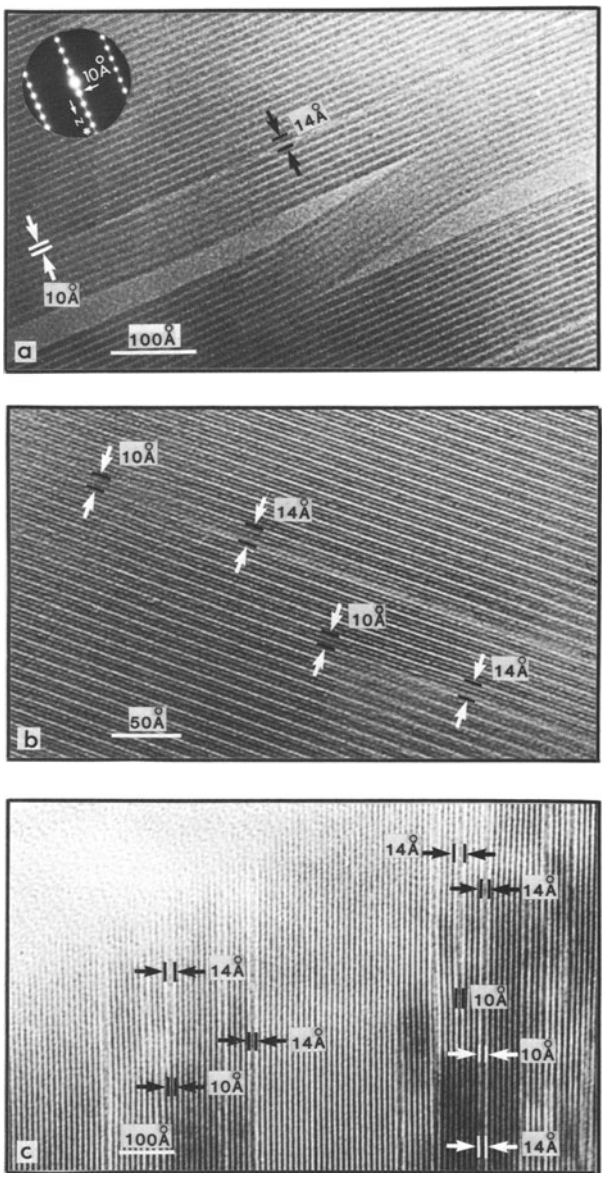


Figure 6. Lattice-fringe images showing (a) conversion of a single biotite layer (10 Å) to vermiculite (14 Å) by direct modification of the existing sheet; (b) conversion of biotite (10 Å) to vermiculite (14 Å). Apparent continuity of the 2:1 biotite layer with the vermiculite layer suggests relatively minor redistribution of components within this layer; (c) conversion of biotite (10 Å) to vermiculite (14 Å) by increase of layer width.

Kaolinite appears to have crystallized onto existing mica sheets (Figure 13) at a time when a substantial amount of space was created by the dissolution of biotite. Unlike vermiculite, kaolinite was not found interstratified with biotite, but only filling larger cavities. The kaolinite layers are subparallel or parallel to biotite and, in later stages of weathering, can be seen as well-formed crystals (see also Figure 15).

https://doi.org/10.1346/CCMN.1988.0360107 Published online by Cambridge University Press

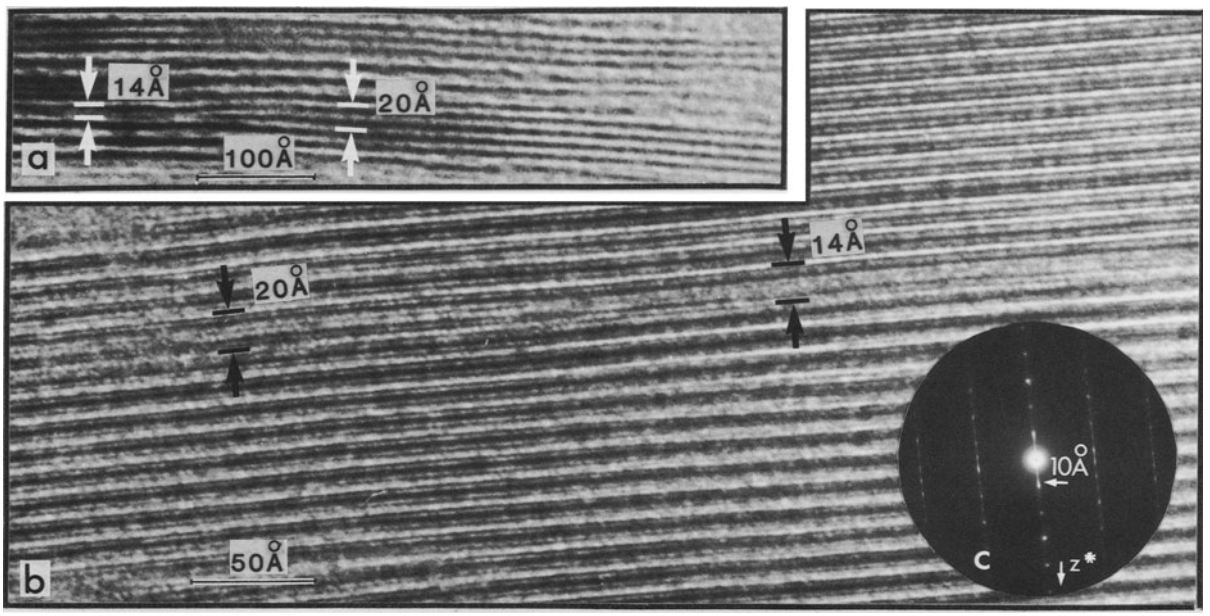


Figure 7. (a), (b) Lattice-fringe images showing conversion of two biotite layers (10 Å) to a single vermiculite layer (14 Å). Gradual thinning of second sheet suggests that vermiculite did not develop at an edge dislocation. Interlayer may form by stripping tetrahedral sheets from this 2:1 layer. (c) Selected area electron diffraction pattern of region shown in (a) and (b).

Goethite appears as a weathering product at the same stage as kaolinite. Initially, narrow (<500 Å wide) regions between strips of phyllosilicates were occupied by iron oxyhydroxides showing a grainy texture (Figure 14). The composition of these regions was determined by qualitative AEM. Larger areas of iron oxyhydroxide (e.g., Figure 15) may also have an irregular linear texture. Some areas show a marked lineation perpendicular to the enclosing phyllosilicate, defining segregations 30 to 40 Å wide (Figure 16). The 10-Å (010)

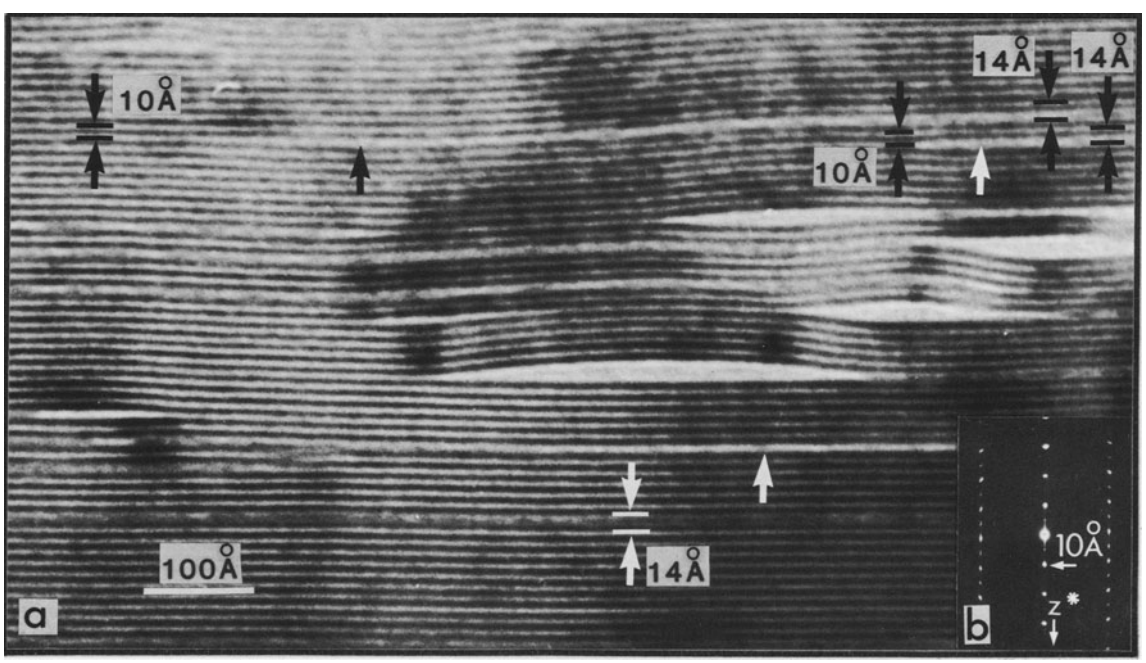


Figure 8. Lattice-fringe images showing (a) brighter interlayer regions (↕) apparently developed as a stage in transformation of biotite to vermiculite, associated locally with an increase in layer width from 10 to 12 Å. Wider gaps where the layers buckle may be beam damage. (b) Selected area electron diffraction pattern.

https://doi.org/10.1346/CCMN.1988.0360107 Published online by Cambridge University Press

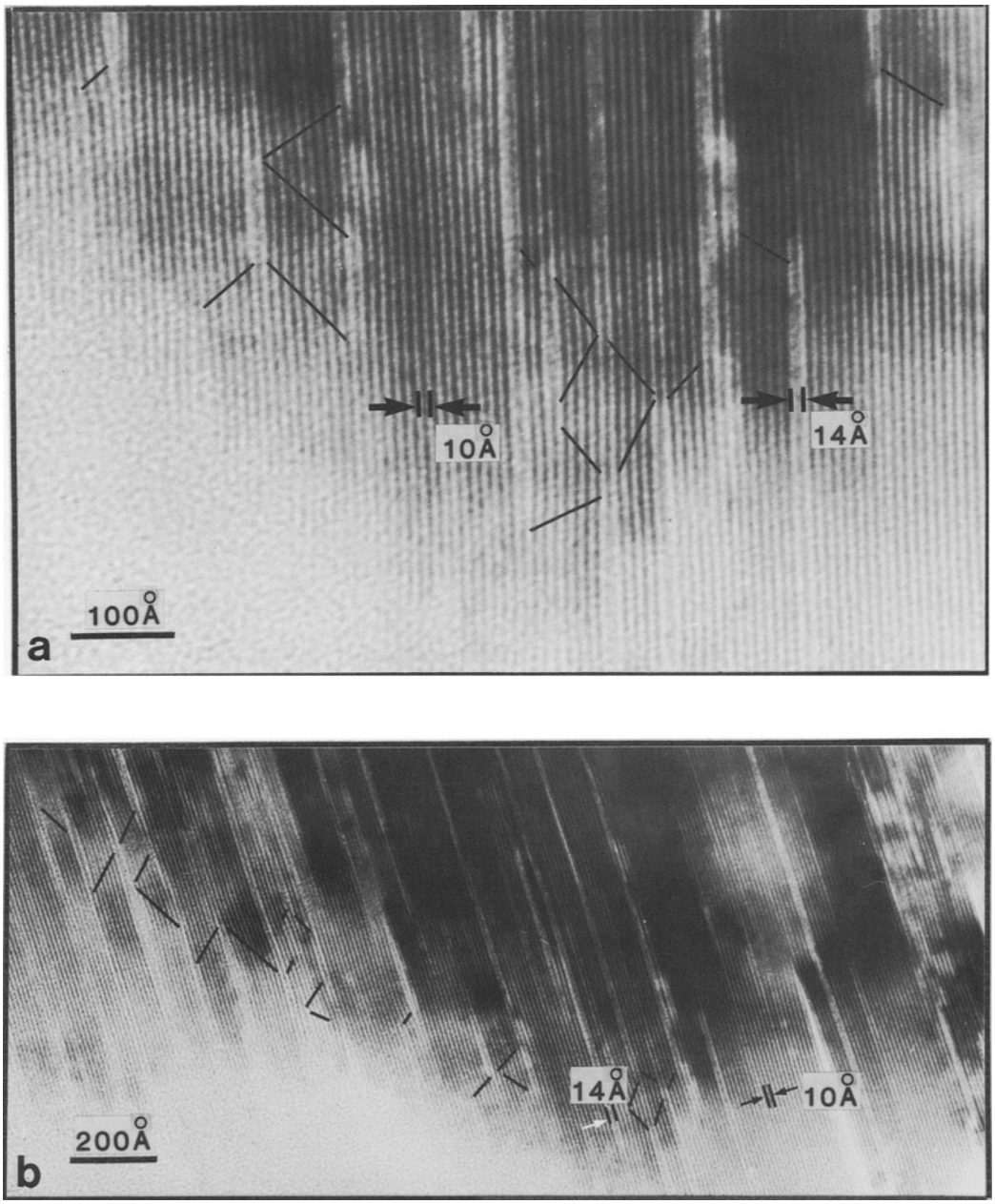


Figure 9. (a) Lattice-fringe images showing paired brucite-like interlayers extending in opposite directions from each end of a flexure in biotite (marked by a short line); (b) lower magnification of (a) illustrating frequency and spacing of vermiculite layers within biotite early in alteration; possible link between flexure of layers and adjacent transformations is more apparent if photograph is viewed at a low angle along the layers.

lattice fringes of goethite were noted in some of these segregations, commonly parallel to their long dimension. Euhedral diamond-shaped ({110} bounded) goethite crystals were also observed at this stage of alteration. The kaolinite : goethite ratio estimated by measuring areas of each mineral on 10 TEMs range from 13 to 28% goethite and average close to a 4:1 kaolinite : goethite ratio.

Halloysite, identified by AEM and by its spherical fabric, commonly coexists with kaolinite and goethite. Spherules of halloysite are as large as 1000 Å in diameter; they occur as fillings of elongate regions between remnant biotite/vermiculite and kaolinite, as do the larger goethite accumulations (Figure 15).

Anatase, iron and manganese oxyhydroxides and halloysite were found concentrated in pits and cracks

https://doi.org/10.1346/CCMN.1988.0360107 Published online by Cambridge University Press

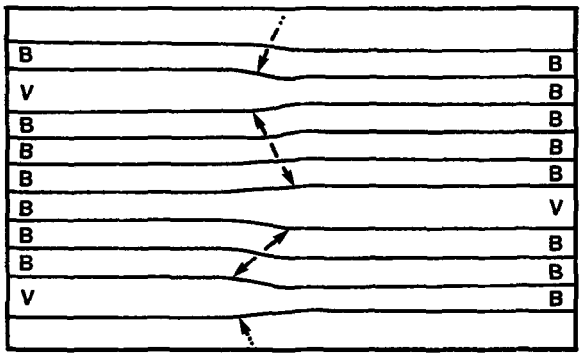


Figure 10. Diagram illustrating proposed link between increased layer thickness due to replacement of biotite by vermiculite and initiation of adjacent transformations. Propagation of adjacent transformations in opposite directions maintains the parallelism of enclosing sheets. Net effect of replacement is to expand the overall volume, apparently into areas where dissolution of the structure has provided space.

in the weathered biotite using SEM and microprobe analysis (Figure 17).

## INTERPRETATION

### *Early stage and biotite-vermiculite stage*

The etch pits observed in the least weathered biotites are probably solution cavities. Their presence in otherwise unaltered biotite suggests leaching at pre-existing points of weaknesses under physiochemical conditions where dissolution was energetically favored over precipitation. Slight expansion of the interlayer region and a lowering of the interlayer electron density (inferred from an increase in brightness as noted in Figure 5) suggests solution of potassium and loss of interlayer cohesion without redeposition of Mg/Fe in the interlayer, and further suggests a dissolution-dominated stage of alteration.

The dissolution stage of weathering apparently provided the space and dissolved ions necessary for the growth of vermiculite. In TEMs, this conversion appears to have proceeded by replacement of K by hydrated interlayer cations which expanded the layer from 10 to 14 Å (Figures 6a–6c).

Each conversion of one biotite unit cell to one vermiculite unit cell requires a volume increase of about 40%. Initially, conversions were apparently infrequent and the volume change was relatively small, accommodated locally by distortion of the surrounding structure. All volume changes were taken up in zones where dissolution had produced space so that the net effect of replacement of biotite by vermiculite was not an increase in the overall volume.

A link between the compression of the structure surrounding the initiation of one vermiculite layer and the termination of a second layer, such as proposed in the drawing in Figure 10, is supported by observations

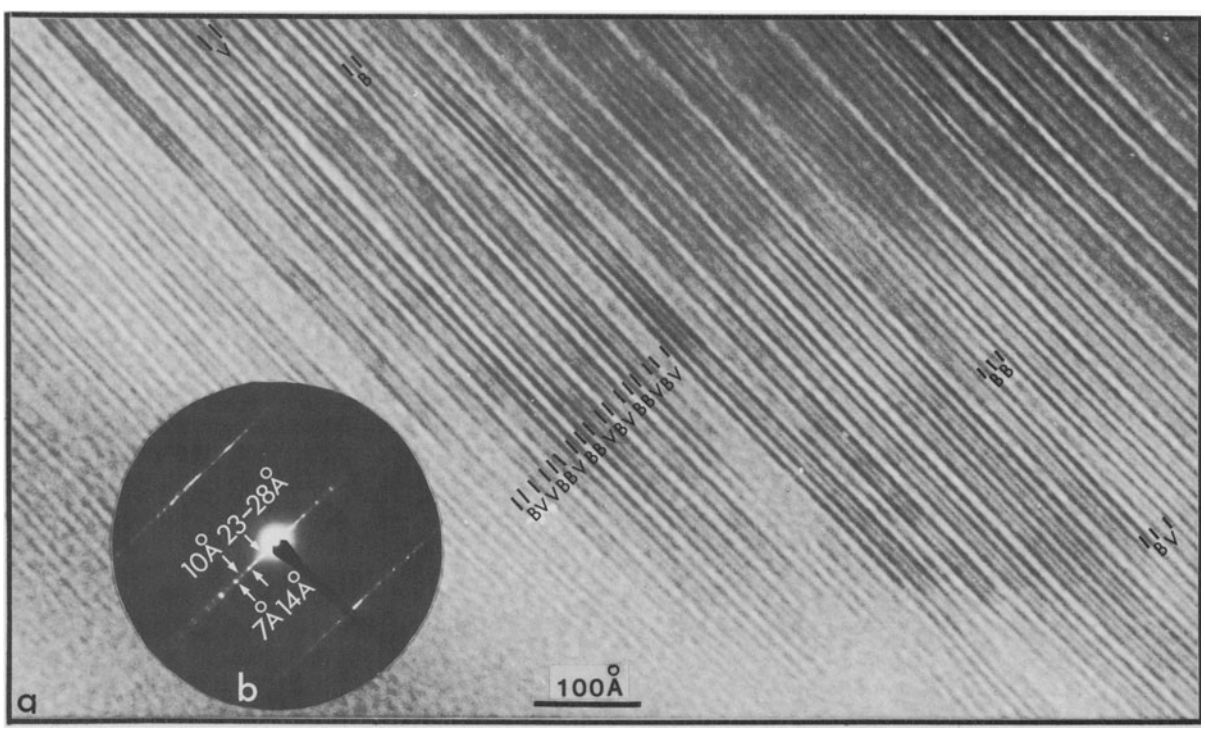


Figure 11. (a) Lattice-fringe images of interlayered biotite and vermiculite illustrating tendency for biotite-vermiculite pairs to form. (b) Selected area electron diffraction pattern from region shown in (a).

https://doi.org/10.1346/CCMN.1988.0360107 Published online by Cambridge University Press

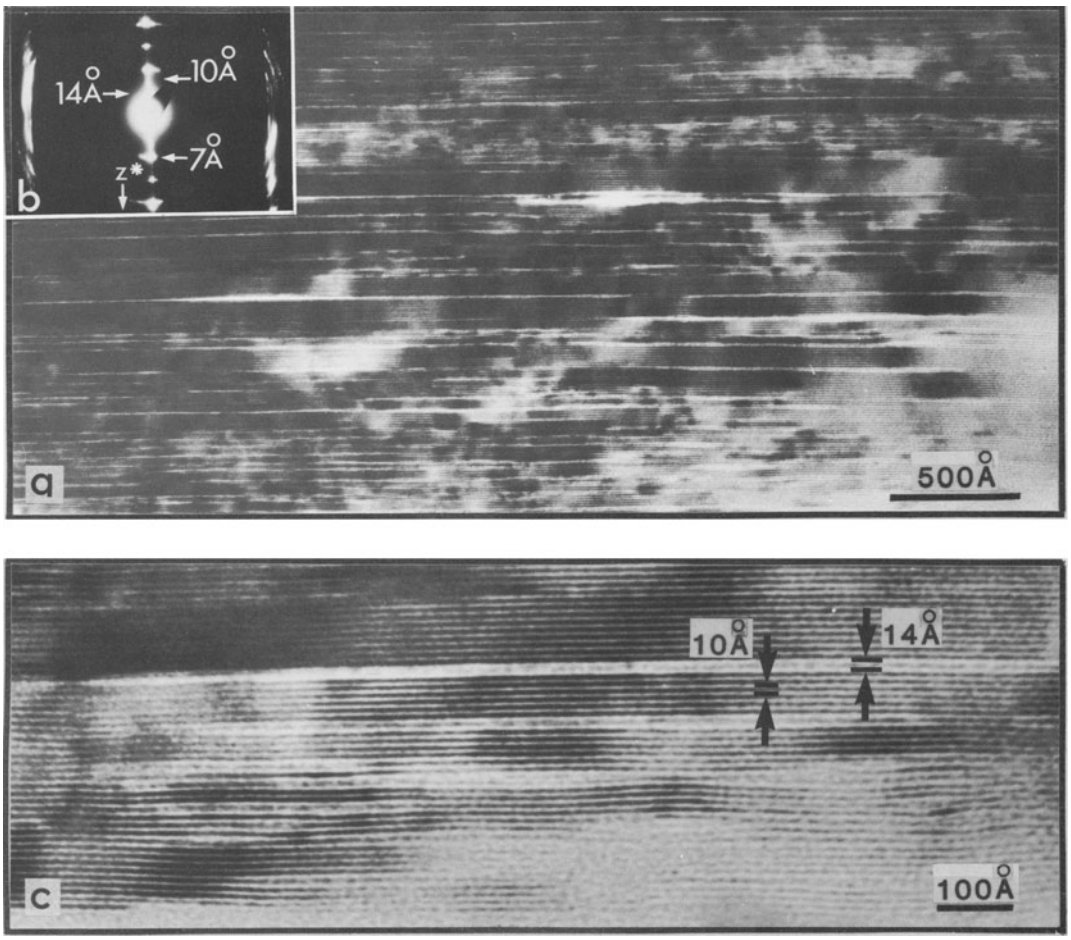


Figure 12. (a) Lattice-fringe images of interlayered biotite and vermiculite illustrating sporadic distribution of single vermiculite layers; low magnification; pale layers are vermiculite. (b) Selected area electron diffraction pattern for an area of altered biotite. Broad 7-Å kaolinite reflections indicate presence of this mineral in zones in biotite. (c) Higher magnification image of (a).

such as those illustrated in Figure 9. The local stress set up at the end of a vermiculite interlayer initially inhibited growth of vermiculite in surrounding biotite and promoted growth of adjacent vermiculite layers in opposite directions. The replacement of the rest of these layers subsequently proceeded with minimal disruption of the surrounding region when compression due to increased layer width was relieved by expansion into gaps produced by dissolution.

Norrish (1973) suggested that the development of regular interstratification is related to the change in OH orientation in the layers adjacent to one from which K had been removed, causing firmer bonding of the K in these layers. TEMs, such as Figure 11, show that vermiculite layers are almost always flanked by biotite layers, suggesting some resistance to alteration in layers adjacent to a vermiculite. From the TEMs, biotite-vermiculite sequences did not apparently develop sequentially outward from an initial vermiculite layer. Rather, vermiculite occurs sporadically throughout the biotite, the average separation between vermiculite layers decreasing as weathering proceeded (Figure 12). Some approximate regularity can be observed in the spacing between vermiculite layers, separations by about four or five biotite layers being common. This longer-range regularity cannot be explained in terms of changes in the OH orientation. The regularity may reflect the distance a second transformation must have been from a vermiculite layer before the stress field around the first transformation had dissipated sufficiently to allow further reactions to proceed.

*Kaolinite-goethite stage*

In the early stages of biotite weathering, limited dissolution appears to have opened some channels which allowed increased access to the weathering agents. The beginning of the kaolinite-goethite stage appears to be marked by rapid oxidation of iron, an extremely abun-

https://doi.org/10.1346/CCMN.1988.0360107 Published online by Cambridge University Press

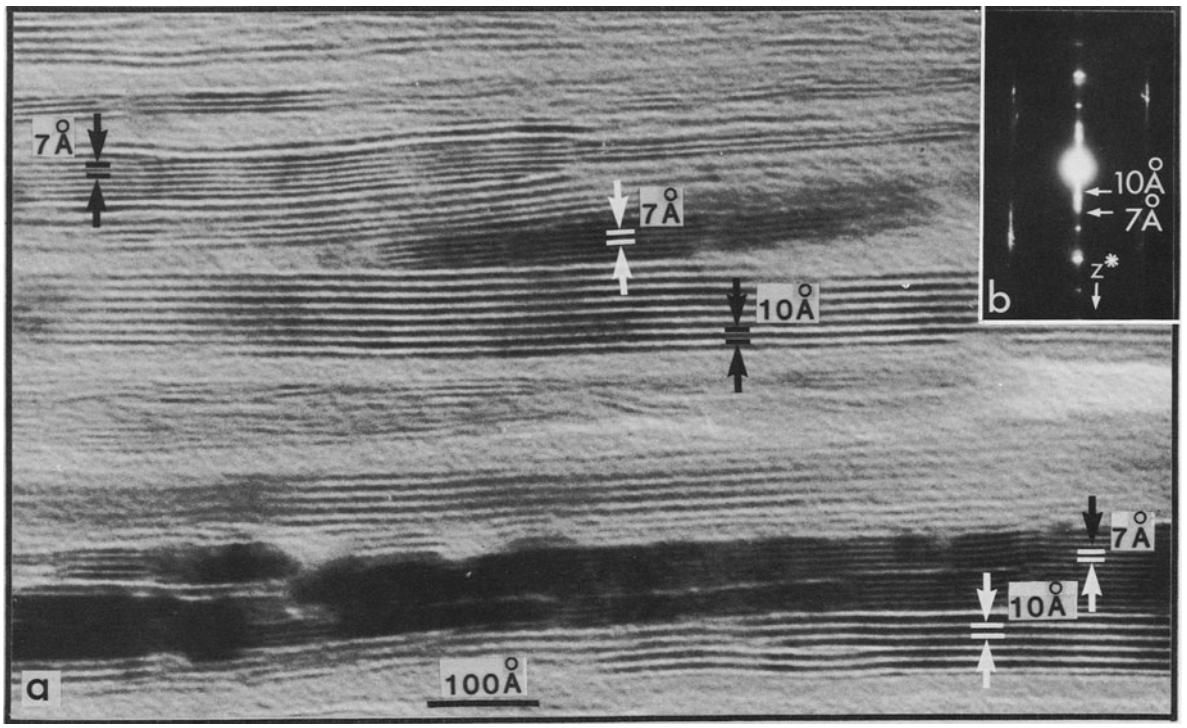


Figure 13. (a) Lattice-fringe images showing packets of 7-Å kaolinite sheets parallel to biotite layers. (b) Selected area electron diffraction pattern, showing orientation relation between kaolinite and biotite.

dant component in this system, comprising about half the octahedral cation population of both biotite and vermiculite. With the destruction of the biotite-vermiculite assemblage, Fe apparently migrated to form segregations of poorly crystalline Fe oxyhydroxide. This material subsequently recrystallized to goethite. Orientations in which (001) goethite is parallel to (001) biotite, and in which (010) goethite is parallel to (001) biotite suggest that the biotite surface exerted some control on the orientation of the goethite. Gilkes and Suddhiprakarn (1979) reported a third orientation, in which (100) goethite is parallel to (001) biotite. These observations therefore indicate that the control was not epitactic.

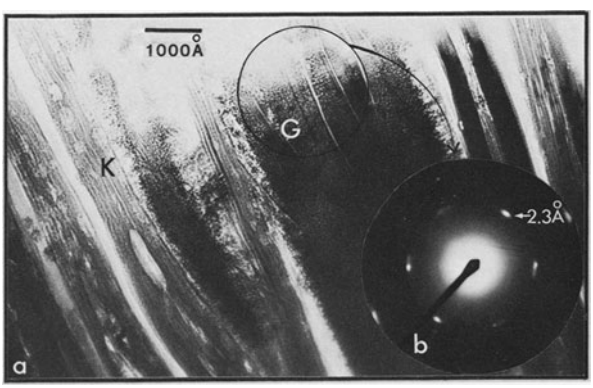


Figure 14. (a) Lattice-fringe images showing very finely oriented crystalline aggregates of goethite (G) enclosed within kaolinite sheets (K). (b) Selected area electron diffraction pattern.

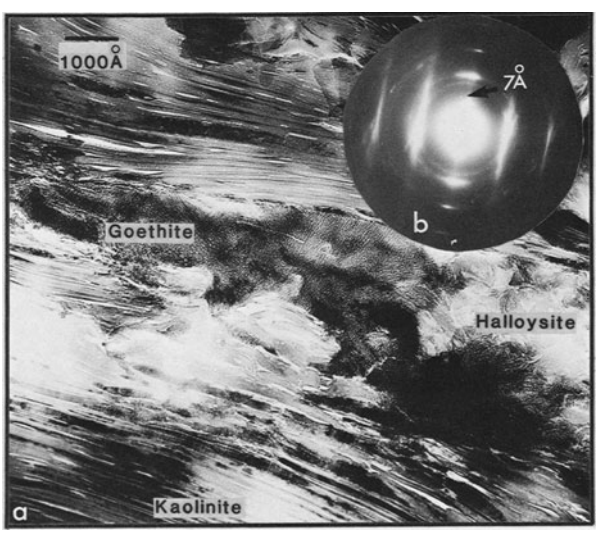


Figure 15. (a) Lattice-fringe images showing lineation developed in finely crystalline goethite between crystals of kaolinite. Some spherical halloysite has developed in space between kaolinite sheets. (b) Selected area electron diffraction pattern containing kaolinite reflections and powder rings produced by goethite.

https://doi.org/10.1346/CCMN.1988.0360107 Published online by Cambridge University Press

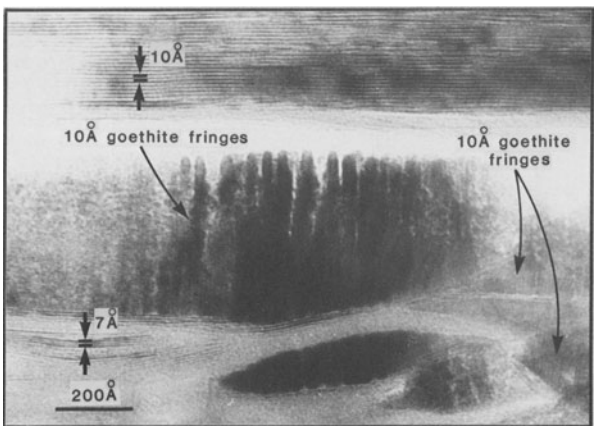


Figure 16. Lattice-fringe images showing oriented laths of goethite and kaolinite (7 Å) within remaining biotite (10 Å).

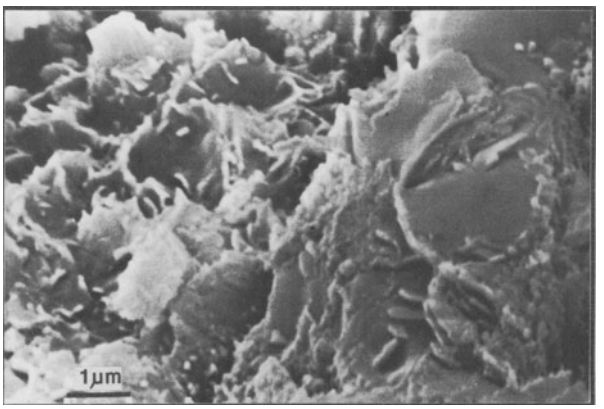


Figure 17. Scanning electron micrograph illustrating Fe-Ti-Mn-rich phase developed in a crack in biotite.

Formation of kaolinite by direct modification of the biotite structure is considered unlikely. First, for this reaction to occur, all Al from both tetrahedral sheets must replace most octahedral cations, Si must replace Al in the tetrahedral sheets, and many components must be removed. Such a reorganization is so dramatic that it would probably not take place without complete destruction of the sheet. Second, kaolinite does not occur as single layers within biotite, but is confined to formation on surfaces, possibly by epitactic crystallization onto existing tetrahedral sheets. On the basis of these observations, it is proposed that under more extreme weathering conditions as biotite was dissolved, kaolinite precipitated epitactically on remaining biotite.

Of the components present within the biotite and vermiculite, K and Si were apparently removed in large amounts in solution as a result of weathering. Mg was hosted temporarily in vermiculite, but was released into solution with the destruction of this mineral. Ti apparently had at least a limited mobility and migrated into pits or cracks where it precipitated to form anatase. Some Fe was released into solution and participated in other weathering reactions in the granite (Banfield, 1985); the remainder recrystallized as goethite.

Table 3. Cation budgets for biotite → vermiculite replacements.

| | 1 Biotite → 1 Vermiculite | | | | |
|---|---|---|---|---|---|
| Cation | Biotite | + | → | Vermiculite | + |
| Si | 5.3 | 0.2 | | 5.5 | 0.3 |
| Al | 3.4 | | | 3.4 | 0 |
| Ti | 0.4 | | | 0.0 | 0.24 |
| Fe | 2.7 | 0.2 | | 2.9 | — |
| Mg | 1.9 | 0.3 | | 2.2 | — |
| K | 2.0 | 0 | | 0 | 2.0 |
| | 2 Biotite → 1 Vermiculite | | | | |
| Cation | 2 Biotite | | → | Vermiculite | + |
| Si | 10.6 | | | 5.5 | 5.3 |
| Al | 6.8 | | | 3.4 | 3.4 |
| Ti | 0.8 | | | 0.0 | 0.8 |
| Fe | 5.4 | | | 2.9 | 2.5 |
| Mg | 3.8 | | | 2.2 | 1.6 |
| K | 4 | | | 0 | 4.0 |

*Reaction chemistry*

The weathering of biotite appears to have taken place very generally in two stages, an initial stage dominated by biotite-vermiculite reactions, and a later stage dominated by the production of kaolinite and goethite. The most commonly observed reaction for the transformation of biotite to vermiculite (mechanism 1) involved loss of interlayer K and introduction of a hydrated Mg-Fe-interlayer, expanding the layer thickness from 10 to 14 Å. Mechanism 2 involved the conversion of two biotite layers to one vermiculite layer, with consequent release of most of the elements of one layer and a thickness decrease from 20 to 14 Å. Table 3 shows the cation budget for both mechanisms for the Bullenbalong (Jindabyne) biotite, selected because it is almost free of chlorite.

Mechanism 1 proceeded at constant Al, releasing K, Si, and Ti and requiring a small amount of Mg and Fe besides water and oxygen. These additional cations were released plentifully by mechanism 2 and, of course, by complete dissolution, such as caused the etch pits shown in Figure 3. No Mg or Fe was required from sources external to the biotite.

The relative timing of the oxidation of Fe and removal of K and the importance of oxidation in initiating the conversion are not clearly indicated by the TEM observations. Oxidation of Fe, however, was probably not the reaction-initiating step and did not control the conversion of biotite to vermiculite. This is supported by the observation that Fe-free phlogopites are converted to vermiculite. Moreover, although the Island Bend biotite is highly oxidized ($Fe^{2+}/Fe^{3+} \approx$

https://doi.org/10.1346/CCMN.1988.0360107 Published online by Cambridge University Press

Table 4. Cation budget for biotite → kaolin + goethite replacement, at constant Al + Fe.

| Cation | Biotite | → | Kaolinite | + | Goethite | + |
|---|---|---|---|---|---|---|
| Si | 5.3 | | 3.5 | | 1.8 | |
| Al | 3.5 | | 3.5 | | | |
| Ti | 0.2 | | 0 | | 0.2 | |
| Fe | 2.6 | | 0.0 | | 2.6 | |
| Mg | 1.9 | | 0.0 | | 1.9 | |
| K | 2.0 | | | | 2.0 | |
| Volume | 490 Å$^3$ | | 290 Å$^3$ | | 90 Å$^3$ | |

2.45) and the Jindabyne biotite highly reduced ($Fe^{2+}/Fe^{3+} \approx 9.92$), the reaction appears to have proceeded by the same mechanisms. The reaction was initiated as $K^+ = H_3O^+$ exchange, which opened up the interlayer and promoted access of oxygen required for the oxidation of octahedral Fe. Oxidation was apparently compensated by redistribution of some octahedral Al (replacing Si in the tetrahedral sheet) and loss of octahedral cations, largely Ti. Substantial Ti cannot be accommodated in the vermiculite structure. This element is released more readily than Mg, Fe, and Al, possibly due to its size and charge.

Little internal evidence exists to provide a basis for the element balance in the conversion of biotite/vermiculite to kaolinite and goethite. TEM photographs show that the products of weathering occupy most of the volume of the original biotite; calculations at constant volume require overall addition of Al and Fe. The budget of Table 4 is based on constant Al and Fe and requires a 20% volume reduction and a kaolinite: goethite volume ratio of slightly more than 3:1, in fair agreement with the measured ratio.

## SUMMARY AND CONCLUSIONS

Biotite weathering, as observed here, can be subdivided generally into two stages. Initially, biotite weathers gradually to interstratified biotite/vermiculite associated with minor quantities of goethite and kaolinite. Even in the earliest stages of weathering, dissolution of biotite plays a significant role in opening up the structure and providing components required for the development of vermiculite. Dissolution is concentrated in zones, apparently where more rapid alteration results in disaggregation of the structure.

Vermiculite develops by direct modification of the biotite structure. This modification may involve the introduction of cations from solution, presumably from adjacent areas where dissolution has occurred, resulting in an increase in layer width from 10 to 14 Å. Less commonly, two biotite layers are replaced by one vermiculite layer, the second biotite layer thinning until it becomes part of the vermiculite structure. This second mechanism requires only the addition of $H_3O^+$ and oxygen. Vermiculite layers that develop in close proximity frequently propagate in opposite directions

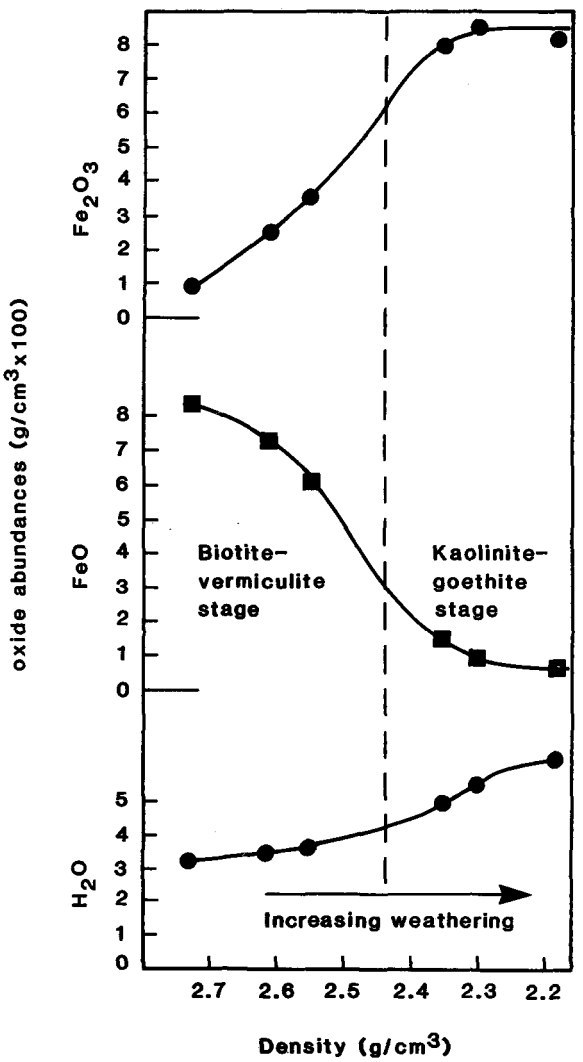


Figure 18. Abundances of FeO, $Fe_2O_3$, and $H_2O+$ in the Bullenbalong Granodiorite weathering profile vs. density, which decreases with increased weathering.

from a common region. This growth appears to be related to the formation of stress fields around volume changes and may serve to promote the early development of some regularity of interlayering. Both mechanisms for the conversion of biotite to vermiculite are associated with a volume change. Although the dominant transformation is associated with a volume increase of about 40%, the volume increase is accommodated locally by distortion of the structure and it is taken up in the abundant space produced by disaggregation and dissolution of the host biotite. Consequently, in the process observed, vermiculitization is not associated with an overall expansion of the structure.

Weathering of biotite to vermiculite appears to have proceeded in the examples studied only to the point where a fairly regularly interstratified 1:1 biotite/ver-

https://doi.org/10.1346/CCMN.1988.0360107 Published online by Cambridge University Press

miculite phase formed. Subsequently only kaolinite and goethite were produced in large amounts. The development of these minerals in abundance corresponded with a period characterized by oxidizing conditions. The change is indicated in chemical data for the profile by a rapid decrease in the abundance of $Fe^{2+}$ and corresponding increase in the abundance of $Fe^{3+}$ (Figure 18).

The second stage, dominated by kaolinite and goethite, is characterized by growth of crystals having an orientation controlled by that of the biotite. Goethite generally develops with its *Y* axis parallel to enclosing sheets, whereas kaolinite forms layers which parallel biotite layers. Unlike vermiculite, which inherits much of its structure and hence orientation from biotite, kaolinite appears to acquire its orientation by epitaxy on the existing silicate structure, crystallizing either from solution or from a noncrystalline precursor.

## ACKNOWLEDGMENTS

We thank B. Hyde of Research School of Chemistry for access to the transmission electron microscopes, P. Barlow, J. Preston, and Nick Ware for technical assistance, B. Chappell for chemical analyses, and D. Goodchild for access to and assistance with the operation of the CSIRO STEM. D. R. Veblen, E. S. Ilton, D. R. Peacor, and B. Velde kindly provided critical reviews of the manuscript.

## REFERENCES

Banfield, J. F. (1985) The mineralogy and chemistry of granite weathering: M.Sc. thesis, Australian National Univ., 130 pp.

Churchman, G. J., Whitton, J. S., Claridge, G. G. C., and Theng, B. K. G. (1984) Intercalation method using formamide for differentiating halloysite from kaolinite: *Clays & Clay Minerals* **32,** 241–248.

Coleman, N. T., Le Roux, F. H., and Cady, I. G. (1963) Biotite-hydrobiotite-vermiculite in soils: *Nature* **198,** 409–410.

Cowley, J. M. and Iijima, S. (1976) The direct imaging of crystal structures: in *Electron Microscopy in Mineralogy,* H.-R. Wenk, ed., Springer-Verlag, Berlin, 123–137.

Gilkes, R. J. and Suddhiprakarn, A. (1979) Biotite in deeply weathered granite. I. Morphologic, mineralogical, and chemical properties. II. The oriented growth of secondary minerals: *Clays & Clay Minerals* **27,** 349–367.

MacEwan, D. M. C. (1953) Cardenite, a trioctahedral montmorillonoid derived from biotite: *Clay Min. Bull.* **2,** 120–126.

Meunier, A. and Velde, B. (1979) Biotite weathering in granites of western France: in *Proc. Int. Clay Conf., Oxford, 1978,* M. M. Mortland and V. C. Farmer, eds., Elsevier, Amsterdam, 405–415.

Norrish, K. (1973) Factors in the weathering of vermiculite: Proc. Int. Clay Conf., Madrid, 1972, J. M. Serratosa, ed. Div. Ciencias C.S.I.C., Madrid, 419–432.

Norrish, K. and Chappell, B. W. (1977) X-ray fluorescence spectroscopy: in *Physical Methods in Determinative Mineralogy,* J. Zussman, ed., Academic Press, New York, 201–272.

Walker, G. F. (1949) The decomposition of biotite in the soil: *Mineral. Mag.* **28,** 693–703.

Wilson, M. J. (1966) The weathering of biotite in some Aberdeenshire soils: *Mineral Mag.* **35,** 1080–1093.

Wilson, M. J. (1970) A study of weathering in a soil derived from a biotite-hornblende rock. I. Weathering of biotite: *Clay Miner.* **8,** 291–303.

*(Received 13 January 1986; accepted 26 August 1987; Ms. 1552)*